Direct Measurement of the Cosmic-Ray Carbon and Oxygen Spectra from 10 GeV/n to 2.2 TeV/n with the Calorimetric Electron Telescope on the International Space Station

O. Adriani,[1,2] Y. Akaike,[3,4,*] K. Asano,[5] Y. Asaoka,[5] M. G. Bagliesi,[6,7] E. Berti,[1,2] G. Bigongiari,[6,7] W. R. Binns,[8] M. Bongi,[1,2] P. Brogi,[6,7] A. Bruno,[9] J. H. Buckley,[8] N. Cannady,[10,11,12] G. Castellini,[13] C. Checchia,[1,2] M. L. Cherry,[14] G. Collazuol,[15,16] K. Ebisawa,[17] H. Fuke,[17] S. Gonzi,[1,2] T. G. Guzik,[14] T. Hams,[10] K. Hibino,[18] M. Ichimura,[19] K. Ioka,[20] W. Ishizaki,[5] M. H. Israel,[8] K. Kasahara,[21] J. Kataoka,[22] R. Kataoka,[23] Y. Katayose,[24] C. Kato,[25] N. Kawanaka,[26,27] Y. Kawakubo,[14] K. Kobayashi,[3,4] K. Kohri,[28] H. S. Krawczynski,[8] J. F. Krizmanic,[10,11,12] J. Link,[10,11,12] P. Maestro,[6,7,†] P. S. Marrocchesi,[6,7] A. M. Messineo,[29,7] J. W. Mitchell,[11] S. Miyake,[30] A. A. Moiseev,[31,11,12] M. Mori,[32] N. Mori,[2] H. M. Motz,[33] K. Munakata,[25] S. Nakahira,[17] J. Nishimura,[17] G. A. de Nolfo,[9] S. Okuno,[18] J. F. Ormes,[34] N. Ospina,[15,16] S. Ozawa,[35] L. Pacini,[1,13,2] F. Palma,[36] P. Papini,[2] B. F. Rauch,[8] S. B. Ricciarini,[13,2] K. Sakai,[10,11,12] T. Sakamoto,[37] M. Sasaki,[31,11,12] Y. Shimizu,[18] A. Shiomi,[38] R. Sparvoli,[39,36] P. Spillantini,[1] F. Stolzi,[6,7] S. Sugita,[37] J. E. Suh,[6,7] A. Sulaj,[6,7] M. Takita,[5] T. Tamura,[18] T. Terasawa,[40] S. Torii,[3] Y. Tsunesada,[41] Y. Uchihori,[42] E. Vannuccini,[2] J. P. Wefel,[14] K. Yamaoka,[43] S. Yanagita,[44] A. Yoshida,[37] and K. Yoshida[21]

(CALET Collaboration)

[1]*Department of Physics, University of Florence, Via Sansone, 1—50019 Sesto, Fiorentino, Italy*
[2]*INFN Sezione di Florence, Via Sansone, 1—50019 Sesto, Fiorentino, Italy*
[3]*Waseda Research Institute for Science and Engineering, Waseda University, 17 Kikuicho, Shinjuku, Tokyo 162-0044, Japan*
[4]*JEM Utilization Center, Human Spaceflight Technology Directorate, Japan Aerospace Exploration Agency, 2-1-1 Sengen, Tsukuba, Ibaraki 305-8505, Japan*
[5]*Institute for Cosmic Ray Research, The University of Tokyo, 5-1-5 Kashiwa-no-Ha, Kashiwa, Chiba 277-8582, Japan*
[6]*Department of Physical Sciences, Earth and Environment, University of Siena, via Roma 56, 53100 Siena, Italy*
[7]*INFN Sezione di Pisa, Polo Fibonacci, Largo B. Pontecorvo, 3—56127 Pisa, Italy*
[8]*Department of Physics and McDonnell Center for the Space Sciences, Washington University, One Brookings Drive, St. Louis, Missouri 63130-4899, USA*
[9]*Heliospheric Physics Laboratory, NASA/GSFC, Greenbelt, Maryland 20771, USA*
[10]*Center for Space Sciences and Technology, University of Maryland, Baltimore County, 1000 Hilltop Circle, Baltimore, Maryland 21250, USA*
[11]*Astroparticle Physics Laboratory, NASA/GSFC, Greenbelt, Maryland 20771, USA*
[12]*Center for Research and Exploration in Space Sciences and Technology, NASA/GSFC, Greenbelt, Maryland 20771, USA*
[13]*Institute of Applied Physics (IFAC), National Research Council (CNR), Via Madonna del Piano, 10, 50019 Sesto, Fiorentino, Italy*
[14]*Department of Physics and Astronomy, Louisiana State University, 202 Nicholson Hall, Baton Rouge, Louisiana 70803, USA*
[15]*Department of Physics and Astronomy, University of Padova, Via Marzolo, 8, 35131 Padova, Italy*
[16]*INFN Sezione di Padova, Via Marzolo, 8, 35131 Padova, Italy*
[17]*Institute of Space and Astronautical Science, Japan Aerospace Exploration Agency, 3-1-1 Yoshinodai, Chuo, Sagamihara, Kanagawa 252-5210, Japan*
[18]*Kanagawa University, 3-27-1 Rokkakubashi, Kanagawa, Yokohama, Kanagawa 221-8686, Japan*
[19]*Faculty of Science and Technology, Graduate School of Science and Technology, Hirosaki University, 3, Bunkyo, Hirosaki, Aomori 036-8561, Japan*
[20]*Yukawa Institute for Theoretical Physics, Kyoto University, Kitashirakawa Oiwakecho, Sakyo, Kyoto 606-8502, Japan*
[21]*Department of Electronic Information Systems, Shibaura Institute of Technology, 307 Fukasaku, Minuma, Saitama 337-8570, Japan*
[22]*Waseda Research Institute for Science and Engineering, Waseda University, 3-4-1 Okubo, Shinjuku, Tokyo 169-8555, Japan*
[23]*National Institute of Polar Research, 10-3, Midori-cho, Tachikawa, Tokyo 190-8518, Japan*
[24]*Faculty of Engineering, Division of Intelligent Systems Engineering, Yokohama National University, 79-5 Tokiwadai, Hodogaya, Yokohama 240-8501, Japan*
[25]*Faculty of Science, Shinshu University, 3-1-1 Asahi, Matsumoto, Nagano 390-8621, Japan*
[26]*Hakubi Center, Kyoto University, Yoshida Honmachi, Sakyo-ku, Kyoto 606-8501, Japan*
[27]*Department of Astronomy, Graduate School of Science, Kyoto University, Kitashirakawa Oiwake-cho, Sakyo-ku, Kyoto 606-8502, Japan*
[28]*Institute of Particle and Nuclear Studies, High Energy Accelerator Research Organization, 1-1 Oho, Tsukuba, Ibaraki 305-0801, Japan*
[29]*University of Pisa, Polo Fibonacci, Largo B. Pontecorvo, 3—56127 Pisa, Italy*

[30]Department of Electrical and Electronic Systems Engineering, National Institute of Technology, Ibaraki College, 866 Nakane, Hitachinaka, Ibaraki 312-8508 Japan
[31]Department of Astronomy, University of Maryland, College Park, Maryland 20742, USA
[32]Department of Physical Sciences, College of Science and Engineering, Ritsumeikan University, Shiga 525-8577, Japan
[33]Faculty of Science and Engineering, Global Center for Science and Engineering, Waseda University, 3-4-1 Okubo, Shinjuku, Tokyo 169-8555, Japan
[34]Department of Physics and Astronomy, University of Denver, Physics Building, Room 211, 2112 East Wesley Ave., Denver, Colorado 80208-6900, USA
[35]Quantum ICT Advanced Development Center, National Institute of Information and Communications Technology, 4-2-1 Nukui-Kitamachi, Koganei, Tokyo 184-8795, Japan
[36]INFN Sezione di Rome "Tor Vergata", Via della Ricerca Scientifica 1, 00133 Rome, Italy
[37]College of Science and Engineering, Department of Physics and Mathematics, Aoyama Gakuin University, 5-10-1 Fuchinobe, Chuo, Sagamihara, Kanagawa 252-5258, Japan
[38]College of Industrial Technology, Nihon University, 1-2-1 Izumi, Narashino, Chiba 275-8575, Japan
[39]University of Rome "Tor Vergata", Via della Ricerca Scientifica 1, 00133 Rome, Italy
[40]RIKEN, 2-1 Hirosawa, Wako, Saitama 351-0198, Japan
[41]Division of Mathematics and Physics, Graduate School of Science, Osaka City University, 3-3-138 Sugimoto, Sumiyoshi, Osaka 558-8585, Japan
[42]National Institutes for Quantum and Radiation Science and Technology, 4-9-1 Anagawa, Inage, Chiba 263-8555, Japan
[43]Nagoya University, Furo, Chikusa, Nagoya 464-8601, Japan
[44]College of Science, Ibaraki University, 2-1-1 Bunkyo, Mito, Ibaraki 310-8512, Japan

(Received 28 July 2020; revised 1 September 2020; accepted 19 November 2020; published 18 December 2020)

In this paper, we present the measurement of the energy spectra of carbon and oxygen in cosmic rays based on observations with the Calorimetric Electron Telescope on the International Space Station from October 2015 to October 2019. Analysis, including the detailed assessment of systematic uncertainties, and results are reported. The energy spectra are measured in kinetic energy per nucleon from 10 GeV/n to 2.2 TeV/n with an all-calorimetric instrument with a total thickness corresponding to 1.3 nuclear interaction length. The observed carbon and oxygen fluxes show a spectral index change of ∼0.15 around 200 GeV/n established with a significance $> 3\sigma$. They have the same energy dependence with a constant C/O flux ratio 0.911 ± 0.006 above 25 GeV/n. The spectral hardening is consistent with that measured by AMS-02, but the absolute normalization of the flux is about 27% lower, though in agreement with observations from previous experiments including the PAMELA spectrometer and the calorimetric balloon-borne experiment CREAM.

DOI: 10.1103/PhysRevLett.125.251102

Introduction.—Direct measurements of charged cosmic rays (CR) provide information on their origin, acceleration, and propagation in the Galaxy. Search for possible charge-dependent cutoffs in the nuclei spectra, hypothesized to explain the knee in the all-particle spectrum [1–4], can be pursued at very large energy by magnetic spectrometers with sufficient rigidity coverage (MDR) or by calorimetric instruments equipped with charge detectors capable of single element resolution. Furthermore, recent observations indicating a spectral hardening in proton and He spectra [5–10] as well as in heavy nuclei spectra [11–14] around a few hundred GeV/n, compelled a revision of the standard paradigm of galactic CR based on diffusive shock acceleration in supernova remnants followed by propagation in galactic magnetic fields, and prompted an intense theoretical activity to interpret these unexpected spectral features [15–26]. The Calorimetric Electron Telescope (CALET) [27–29] is a space-based instrument optimized for the measurement of the all-electron spectrum [30,31], which can also measure individual chemical elements in CR from proton to iron and above in the energy range up to ∼1 PeV. CALET recently confirmed the spectral hardening in the proton spectrum by accurately measuring its power-law spectral index over the wide energy range from 50 GeV to 10 TeV [32].

In this Letter, we present a new direct measurement of the CR carbon and oxygen spectra from 10 GeV/n to 2.2 TeV/n, based on the data collected by CALET from October 13, 2015 to October 31, 2019 aboard the International Space Station (ISS).

CALET instrument.—CALET consists of a charge detector (CHD), a finely segmented preshower imaging calorimeter (IMC), and a total absorption calorimeter (TASC). CHD is comprised of two hodoscopes made of 14 plastic scintillator paddles each, arranged in orthogonal layers (CHDX, CHDY). The CHD can resolve individual chemical elements from $Z = 1$ to $Z = 40$, with excellent charge resolution. The IMC consists of 7 tungsten plates

inserted between eight double layers of 1 mm^2 cross-section scintillating fibers, arranged in belts along orthogonal directions and individually read out by multianode photomultiplier tubes. Its fine granularity and imaging capability allow an accurate particle tracking and an independent charge measurement via multiple samples of the particle ionization energy loss (dE/dx) in each fiber. The TASC is a homogeneous calorimeter made of lead-tungstate ($PbWO_4$) bars arranged in 12 layers. The crystal bars in the top layers are read out by photomultiplier tubes, while a dual photodiode–avalanche-photodiode (PD–APD) system is used for each channel in the remaining layers. A dynamic range of more than 6 orders of magnitude is covered using a front-end electronics with dual gain range for each photosensor. The total thickness of the instrument is equivalent to 30 radiation lengths and 1.3 nuclear interaction lengths. A more complete description of the instrument can be found in the Supplemental Material of Ref. [30]. CALET was launched on August 19, 2015 and installed on the Japanese Experiment Module Exposure Facility of the ISS. The on-orbit commissioning phase aboard the ISS was successfully completed in the first days of October 2015, and since then the instrument has been taking science data continuously [33].

Data analysis.—We have analyzed flight data (FD) collected in 1480 days of CALET operation. The total observation live time for the high-energy (HE) shower trigger is $T = 3.00 \times 10^4$ h, corresponding to 84.5% of total observation time.

Raw data are corrected for nonuniformity in light output, time and temperature dependence, and gain differences among the channels. The latter are individually calibrated on orbit by using penetrating proton and He particles, selected by a dedicated trigger mode [34,35]. After calibrations, each CR particle track is reconstructed and a charge and an energy are assigned for each event.

Monte Carlo (MC) simulations, reproducing the detailed detector configuration, physics processes, as well as detector signals, are based on the EPICS simulation package [36,37] and employ the hadronic interaction model DPMJET-III [38]. An independent analysis based on FLUKA [39,40] is also performed to assess the systematic uncertainties.

The CR particle direction and its entrance point in the instrument are reconstructed by a track finding and fitting algorithm based on a combinatorial Kalman filter [41], which is able to identify the incident track in the presence of a background of secondary tracks backscattered from TASC. The angular resolution is ~0.1° for C and O nuclei and the spatial resolution on the determination of the impact point on CHD is ~220 μm.

The identification of the particle charge Z is based on the measurements of the ionization deposits in CHD and IMC. The particle trajectory is used to identify the CHD paddles and IMC fibers traversed by the primary particle and to determine the path length correction to be applied to the signals to extract the dE/dx samples. Three independent dE/dx measurements are obtained, one for each CHD layer and the third by averaging the samples (at most eight) along the track in the top half of IMC. Calibration curves of dE/dx are built by fitting FD subsets for each nuclear species to a function of Z^2 by using a "halo" model [42]. These curves are then used to reconstruct three charge values (Z_{CHDX}, Z_{CHDY}, Z_{IMC}) from the measured dE/dx on an event-by-event basis [43]. For high-energy showers, the charge peaks are corrected for the systematical shift to higher values (up to $0.15e$) with respect to the nominal charge positions, due to the large amount of shower particle tracks backscattered from TASC whose signals add up to the primary particle ionization signal. A charge distribution obtained by averaging Z_{CHDX} and Z_{CHDY} is shown in Fig. S1 of the Supplemental Material [44]. The charge resolution σ_Z is ~$0.15e$ (charge unit) for CHD and ~$0.24e$ for IMC, respectively, in the elemental range from B to O.

The shower energy E_{TASC} of each event is calculated as the sum of the energy deposits of all the TASC channels, after stitching the adjacent gain ranges of each PD-APD. The energy response of TASC was studied in a beam test carried out at CERN-SPS in 2015 with accelerated ion fragments of 13, 19 and 150 GeV/c momentum per nucleon [45]. The MC simulations were tuned using the beam test results as described in the energy measurement section of the Supplemental Material [44].

Carbon and oxygen candidates are identified among events selected by the onboard HE shower trigger, based on the coincidence of the summed signals of the last two IMC layers in each view and the top TASC layer (TASCX1). Consistency between MC and FD for triggered events is obtained by an off-line trigger with higher thresholds [50 and 100 times a minimum ionizing particle (MIP) signal for IMC and TASC, respectively] than the onboard trigger removing possible effects due to residual nonuniformity of the detector gain. In order to reject possible events triggered by particles entering the TASC from lateral sides or with significant lateral leakage, the energy deposits in the first TASC layer (TASCX1) and in all the lateral bars are required to be less than 40% of E_{TASC}. Late-interacting events in the bottom half of TASC are rejected by requiring that the energy deposit in the last layer is $< 0.4 \times E_{\mathrm{TASC}}$, and the layer, where the longitudinal shower development reaches 20% of E_{TASC}, occurs in the upper half of TASC.

Events with one well-fitted track crossing the whole detector from CHD top to the TASC bottom layer and at least 2 cm away from the edges in TASCX1 are then selected. The fiducial geometrical factor for this category of events is $S\Omega \sim 510$ cm^2 sr, corresponding to about 50% of the total CALET acceptance.

Carbon and oxygen candidates are selected by applying window cuts, centered on the nominal charge values ($Z = 6$, 8), of half-width $0.4e$ for Z_{CHDX} and Z_{CHDY}, and $2\sigma_Z$ for Z_{IMC}, respectively. Particles undergoing a

charge-changing nuclear interaction in the upper part of the instrument (Fig. S2 of the Supplemental Material [44]) are removed by the three combined charge selections and by requiring the consistency, within 30%, between the mean values of dE/dx measurements in the first four layers in each IMC view.

Distributions of E_{TASC} for C and O selected candidates are shown in Fig. S3 of Supplemental Material [44], corresponding to 6.154×10^5 C and 1.047×10^6 O events, respectively. In order to take into account the relatively limited energy resolution (Fig. S4 of the Ref. [44]) energy unfolding is necessary to correct for bin-to-bin migration effects. In this analysis, we used the Bayesian approach [46] implemented in the RooUnfold package [47] in ROOT [48]. Each element of the response matrix represents the probability that primary nuclei in a certain energy interval of the CR spectrum produce an energy deposit in a given bin of E_{TASC}. The response matrix (Fig. S5 of the Supplemental Material [44]) is derived using MC simulation after applying the same selection procedure as for FD.

The energy spectrum is obtained from the unfolded energy distribution as follows:

$$\Phi(E) = \frac{N(E)}{\Delta E \varepsilon(E) S \Omega T}, \tag{1}$$

$$N(E) = U[N_{\mathrm{obs}}(E_{\mathrm{TASC}}) - N_{bg}(E_{\mathrm{TASC}})], \tag{2}$$

where ΔE denotes energy bin width, E the particle kinetic energy, calculated as the geometric mean of the lower and upper bounds of the bin, $N(E)$ is the bin content in the unfolded distribution, $\varepsilon(E)$ the total selection efficiency (Fig. S6 of the Supplemental Material [44]), $U()$ the unfolding procedure, $N_{\mathrm{obs}}(E_{\mathrm{TASC}})$ the bin content of observed energy distribution (including background), $N_{\mathrm{bg}}(E_{\mathrm{TASC}})$ the bin content of background events in the observed energy distribution. Background contamination from different nuclear species misidentified as C or O is shown in Fig. S3 of the Supplemental Material [44]. A contamination fraction $N_{\mathrm{bg}}/N_{\mathrm{obs}} < 0.1\%$ is found in all energy bins with $E_{\mathrm{TASC}} < 10^3$ GeV, and between 0.1% and 1% for $E_{\mathrm{TASC}} > 10^3$ GeV.

Systematic uncertainties.—In this analysis, dominant sources of systematic uncertainties include trigger efficiency, energy response, event selection, unfolding procedure, and the MC model. HE trigger efficiency as a function of E_{TASC} was inferred from the data taken with a minimum bias trigger. HE efficiency curves for C and O are consistent with predictions from MC simulations, as shown in Fig. S7 of the Supplemental Material [44]. In order to study the flux stability against off-line trigger efficiency, the threshold applied to TASCX1 signal was scanned between 100 and 150 MIP signal. The corresponding systematic errors range between −4.2% (−3.1%) and 3.7% (7.3%) for C (O) depending on the energy bin.

The systematic error related to charge identification was studied by varying the width of the window cuts between $0.35e$ and $0.45e$ for CHD and between $1.75\sigma_Z$ and $2.2\sigma_Z$ for IMC. That results in a flux variation depending on the energy bin, which is less than 1% below 250 GeV/n and few percent above. The ratio of events selected by IMC charge cut to the ones selected with CHD in different E_{TASC} intervals turned out to be consistent in FD and MC. Possible inaccuracy of track reconstruction could affect the determination of the geometrical acceptance. The contamination due to off-acceptance events which are misreconstructed in the fiducial acceptance was estimated with MC to be ∼1% at 10 GeV/n and decrease to less than 0.1% above 60 GeV/n. To investigate the uncertainty in the definition of the acceptance, restricted acceptance (up to 20% of nominal one) regions were also studied. The corresponding fluxes are consistent within statistical fluctuations.

A different tracking procedure, described in Ref. [49], was also used to study possible systematic uncertainties in tracking efficiency. Results are consistent with those obtained with the Kalman filter algorithm, hence we consider negligible this source of systematic error.

The uncertainty in the energy scale is ±2% and depends on the accuracy of the beam test calibration. It causes a rigid shift of the measured energies, affecting the absolute normalization of the C and O spectra by $^{+2.6\%}_{-2.8\%}$, but not their shape. As the beam test model was not identical to the instrument now in orbit, the difference in the spectrum obtained with either configuration was modeled and included in the systematic error.

Other energy-independent systematic uncertainties affecting the normalization include live time (3.4%, as explained in the Supplemental Material of Ref. [30]) and long-term stability of the charge measurements (<0.4%). and energy (< 3%) measurements.

The uncertainties due to the unfolding procedure were evaluated by using different response matrices, computed by varying the spectral index (between −2.9 and −2.5) of the generation spectrum of MC simulations, and the singular value deconvolution method, instead of the Bayesian approach, in RooUnfold software [47].

Since it is not possible to validate MC simulations with beam test data in the high-energy region, a comparison between different MC models, i.e., EPICS and FLUKA, was performed. We found that the total selection efficiencies for C and O determined with the two models are in agreement within < 1.5% over the whole energy range, but the energy response matrices differ significantly in the low and high energy regions. The resulting fluxes show maximum discrepancies of 9% (7.8%) and 9.2% (12.2%), respectively, in the first and last energy bin for C (O), while they are consistent within 6.6% (6.2%) elsewhere. This is the dominant source of systematic uncertainties.

Materials traversed by nuclei in IMC are mainly composed of carbon, aluminum, and tungsten. Possible uncertainties in the inelastic cross sections in simulations or discrepancies in the material description might affect the flux normalization. We have checked that hadronic interactions are well simulated in the detector, by measuring the survival probabilities of C and O nuclei at different depths in IMC, as described in the Supplemental Material [44]. The survival probabilities are in agreement with MC prediction within $< 1\%$ (Fig. S8 of the Ref. [44]). Background contamination from different nuclear species estimated with FLUKA and EPICS simulations differ by less than 1%.

The energy dependence of all the systematic uncertainties for C and O is shown in Fig. S9 of the Supplemental Material [44]. The total systematic error is computed as the sum in quadrature of all the sources of systematics in each energy bin.

Results.—The energy spectra of carbon and oxygen and their flux ratio measured with CALET in an energy range from 10 GeV/n to 2.2 TeV/n are shown in Fig. 1, where current uncertainties that include statistical and systematic errors are bounded within a gray band. CALET spectra are compared with results from space-based [14,50–53] and balloon-borne [54–57] experiments. The measured C and O fluxes and flux ratio with statistical and systematic errors are tabulated in Tables I, II, and III of the Supplemental Material [44]. Our spectra are consistent with PAMELA [52] and most previous experiments [50,51,55–57], but the absolute normalization is in tension with AMS-02 [14]. However we notice that C/O ratio [Fig. 1(c)] is consistent with the one measured by AMS-02. In Fig. S11 of the Supplemental Material [44], it is shown that CALET and AMS-02 C and O spectra have very similar shapes but they differ in the absolute normalization, which is lower for CALET by about 27% for both C and O. Figure 2 shows the fits to CALET carbon and oxygen data with a double power-law function [DPL, Eq. (S1) in Supplemental Material [44]] above 25 GeV/n. A single power-law function [SPL, Eq. (S2) in Ref. [44]] fitted to data in the energy range $[25, 200]$ GeV/n and extrapolated above 200 GeV/n is also shown for comparison. The effect of systematic uncertainties in the measurement of the energy spectrum is modeled in the χ^2 minimization function with a set of 6 nuisance parameters as explained in detail in the Supplemental Material [44]. The DPL fit to the C spectrum yields a spectral index $\gamma = -2.663 \pm 0.014$ at energies below the transition region $E_0 = (215 \pm 54)$ GeV/n and a spectral index increase $\Delta\gamma = 0.166 \pm 0.042$ above, with $\chi^2/\text{d.o.f.} = 9.0/8$. For oxygen, the fit yields $\gamma = -2.637 \pm 0.009$, $E_0 = (264 \pm 53)$ GeV/n, $\Delta\gamma = 0.158 \pm 0.053$, with $\chi^2/\text{d.o.f.} = 3.0/8$. SPL fits to CALET carbon and oxygen data above 25 GeV/n are shown in Figs. S12 and S13 of the Supplemental Material [44]. They give $\gamma = -2.626 \pm 0.010$ with $\chi^2/\text{d.o.f.} = 27.5/10$ for C, and $\gamma = -2.622 \pm 0.008$ with $\chi^2/\text{d.o.f.} = 15.9/10$ for O, respectively. A frequentist test statistic $\Delta\chi^2$ is computed from the difference in χ^2 between the fits with SPL and DPL functions. For carbon (oxygen), $\Delta\chi^2 = 18.5$ (12.9) with 2 d.o.f. (i.e., the number of additional free parameters in DPL fit with respect to SPL fit) implies that the significance of the hardening of the C(O) spectrum exceeds the 3σ level. We also checked that the spectral hardening is not an artifact of the energy binning and unfolding, by increasing the bin width by a factor 2.5 as shown in Fig. S14 of the Supplemental Material [44]. The resulting flux difference is negligible when compared with our estimated systematic uncertainties.

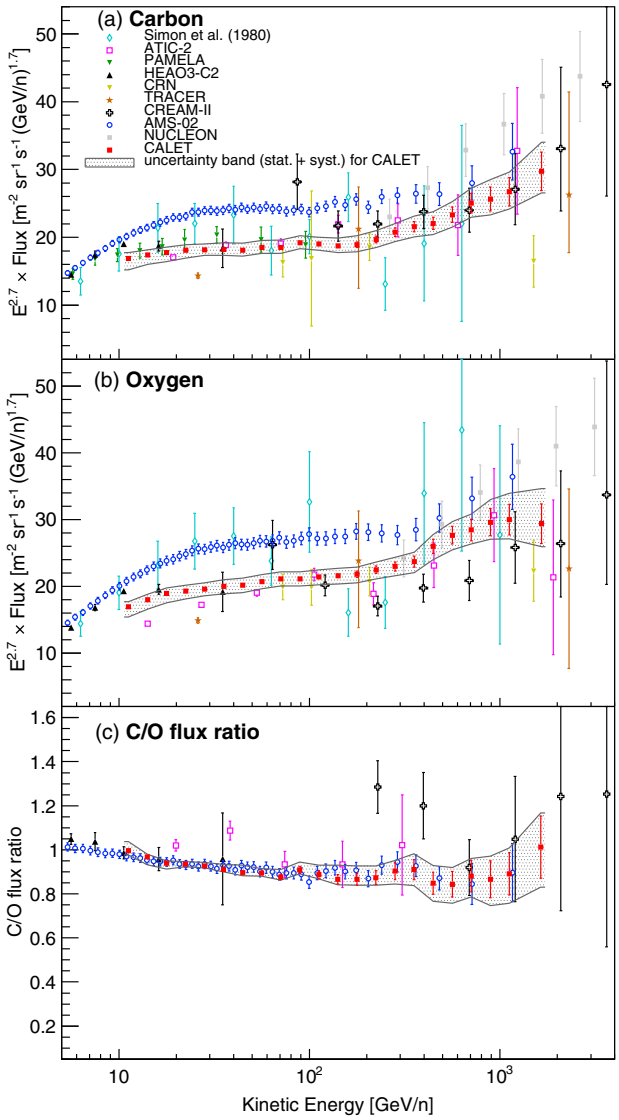

FIG. 1. CALET (a) carbon and (b) oxygen flux (multiplied by $E^{2.7}$) and (c) ratio of carbon to oxygen fluxes, as a function of kinetic energy E. Error bars of CALET data (red) represent the statistical uncertainty only, while the gray band indicates the quadratic sum of statistical and systematic errors. Also plotted are other direct measurements [14,50–57]. An enlarged version of the figure is available as Fig. S10 in the Supplemental Material [44].

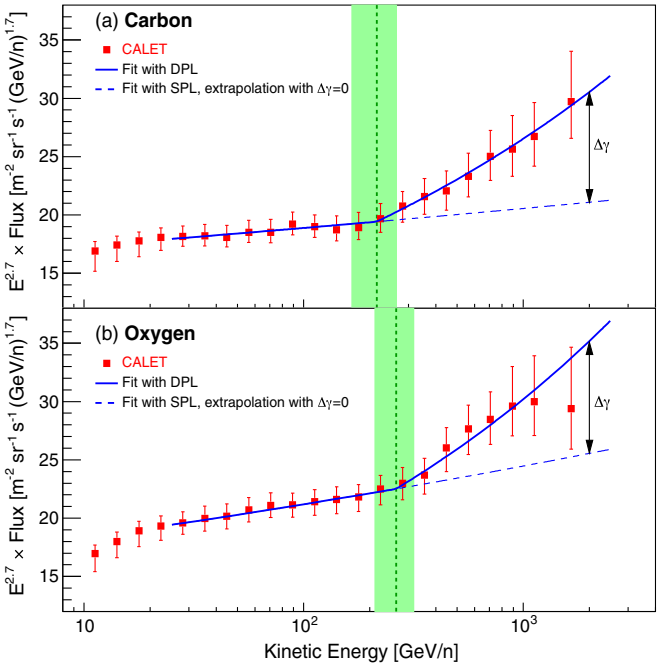

FIG. 2. Fit of the CALET (a) C and (b) O energy spectra with a DPL function (blue line) in the energy range $[25, 2000]$ GeV/n. The flux is multiplied by $E^{2.7}$ where E is the kinetic energy per nucleon. Error bars of CALET data points represent the sum in quadrature of statistical and systematic uncertainties. The dashed blue lines represent the extrapolation of a SPL function fitted to data in the energy range $[25, 200]$ GeV/n. $\Delta\gamma$ is the change of the spectral index above the transition energy E_0, represented by the vertical green dashed line. The error interval for E_0 from the DPL fit is shown by the green band.

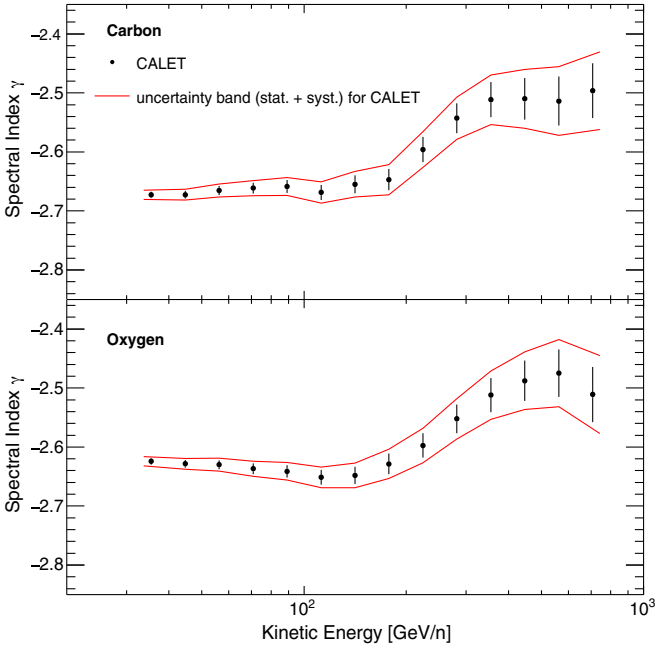

FIG. 3. Energy dependence of the spectral index calculated within a sliding energy window for CALET (a) C and (b) O data. The spectral index is determined for each bin by fitting the data using ± 3 bins. Red curves indicate the uncertainty range including systematic errors.

In order to study the energy dependence of the spectral index in a model independent way, the spectral index γ is calculated by a fit of $d[\log(\Phi)]/d[\log(E)]$ in energy windows centered in each bin and including the neighbor ± 3 bins. The results in Fig. 3 show that carbon and oxygen fluxes harden in a similar way above a few hundred GeV/n. The carbon to oxygen flux ratio is well fitted to a constant value of 0.911 ± 0.006 above 25 GeV/n (Fig. S15 of the Supplemental Material [44]), indicating that the two fluxes have the same energy dependence.

Conclusion.—With a calorimetric apparatus in low Earth orbit, CALET has measured the energy spectra of carbon and oxygen nuclei in CR and their flux ratio from 10 GeV/n to 2.2 TeV/n. Our observations allow to exclude a single power law spectrum for C and O by more than 3σ; they show a spectral index increase $\Delta\gamma = 0.166 \pm 0.042$ for C and $\Delta\gamma = 0.158 \pm 0.053$ for O above 200 GeV/n, and the same energy dependence for C and O fluxes with a constant C/O flux ratio 0.911 ± 0.006 above 25 GeV/n. These results are consistent with the ones reported by AMS-02. However the absolute normalization of our data is significantly lower than AMS-02, but in agreement with previous experiments. Improved statistics and refinement of the analysis with additional data collected during the lifetime of the mission will allow to extend the measurements at higher energies and improve the spectral analysis, contributing to a better understanding of the origin of the spectral hardening.

We gratefully acknowledge JAXA's contributions to the development of CALET and to the operations onboard the International Space Station. We also wish to express our sincere gratitude to Agenzia Spaziale Italiana (ASI) and NASA for their support of the CALET project. This work was supported in part by JSPS Grant-in-Aid for Scientific Research (S) No. 26220708 and No. 19H05608, JSPS Grant-in-Aid for Scientific Research (B) No. 17H02901, and by the MEXT-Supported Program for the Strategic Research Foundation at Private Universities (2011-2015) (No. S1101021) at Waseda University. The CALET effort in Italy is supported by ASI under agreement 2013-018-R.0 and its amendments. The CALET effort in the United States is supported by NASA through Grants No. NNX16AB99G, No. NNX16AC02G, and No. NNH14ZDA001N-APRA-0075.

*yakaike@aoni.waseda.jp
†maestro@unisi.it

[1] P. O. Lagage and C. J. Cesarsky, Astron. Astrophys. **125**, 249 (1983), http://adsabs.harvard.edu/full/1983A%26A...125..249L.
[2] E. G. Berezhko, Astropart. Phys. **5**, 367 (1996).
[3] J. R. Hörandel, Astropart. Phys. **21**, 241 (2004).

[4] E. Parizot, A. Marcowith, E. van der Swaluw, A. M. Bykov, and V. Tatischeff, Astron. Astrophys. **424**, 747 (2004).
[5] M. Aguilar *et al.* (AMS Collaboration), Phys. Rev. Lett. **114**, 171103 (2015).
[6] M. Aguilar *et al.* (AMS Collaboration), Phys. Rev. Lett. **115**, 211101 (2015).
[7] O. Adriani *et al.* (PAMELA Collaboration), Science **332**, 69 (2011).
[8] Y. S. Yoon *et al.* (CREAM Collaboration), Astrophys. J. **728**, 122 (2011).
[9] Y. S. Yoon *et al.* (CREAM Collaboration), Astrophys. J. **839**, 5 (2017).
[10] Q. An *et al.* (DAMPE Collaboration), Sci. Adv. **5**, eaax3793 (2019).
[11] M. Ave *et al.* (TRACER Collaboration), Astrophys. J. **697**, 106 (2009).
[12] A. Obermeier *et al.* (TRACER Collaboration), Astrophys. J. **742**, 14 (2011).
[13] H. S. Ahn *et al.* (CREAM Collaboration), Astrophys. J. Lett. **714**, L89 (2010).
[14] M. Aguilar *et al.* (AMS Collaboration), Phys. Rev. Lett. **119**, 251101 (2017).
[15] P. Serpico, Proc. Sci., ICRC2015 (**2015**) 009, https://pos.sissa.it/236/009/pdf.
[16] M. A. Malkov, P. H. Diamond, and R. Z. Sagdeev, Phys. Rev. Lett. **108**, 081104 (2012).
[17] G. Bernard, T. Delahaye, Y.-Y. Keum, W. Liu, P. Salati, and R. Taillet, Astron. Astrophys. **555**, A48 (2013).
[18] N. Tomassetti, Astrophys. J. Lett. **752**, L13 (2012).
[19] L. O. Drury, Mon. Not. R. Astron. Soc. **415**, 1807 (2011).
[20] P. Blasi, E. Amato, and P. D. Serpico, Phys. Rev. Lett. **109**, 061101 (2012).
[21] C. Evoli, P. Blasi, G. Morlino, and R. Aloisio, Phys. Rev. Lett. **121**, 021102 (2018).
[22] Y. Ohira and K. Ioka, Astrophys. J. Lett. **729**, L13 (2011).
[23] Y. Ohira, N. Kawanaka, and K. Ioka, Phys. Rev. D **93**, 083001 (2016).
[24] A. Vladimirov, G. Johannesson, I. Moskalenko, and T. Porter, Astrophys. J. **752**, 68 (2012).
[25] V. Ptuskin, V. Zirakashvili, and E. S. Seo, Astrophys. J. **763**, 47 (2013).
[26] S. Thoudam and J. R. Hörandel, Astron. Astrophys. **567**, A33 (2014).
[27] S. Torii and P. S. Marrocchesi (CALET Collaboration), Adv. Space Res. **64**, 2531 (2019).
[28] S. Torii (CALET Collaboration), Proc. Sci., ICRC2017 (**2017**) 1092, https://pos.sissa.it/301/1092/pdf.
[29] Y. Asaoka (CALET Collaboration), Proc. Sci., ICRC2019 (**2019**) 001, https://pos.sissa.it/358/001/pdf.
[30] O. Adriani *et al.* (CALET Collaboration), Phys. Rev. Lett. **119**, 181101 (2017).
[31] O. Adriani *et al.* (CALET Collaboration), Phys. Rev. Lett. **120**, 261102 (2018).
[32] O. Adriani *et al.* (CALET Collaboration), Phys. Rev. Lett. **122**, 181102 (2019).
[33] Y. Asaoka *et al.* (CALET Collaboration), Astropart. Phys. **100**, 29 (2018).
[34] Y. Asaoka *et al.* (CALET Collaboration), Astropart. Phys. **91**, 1 (2017).
[35] T. Niita *et al.* (CALET Collaboration), Adv. Space Res. **55**, 2500 (2015).
[36] K. Kasahara, in *Proceedings of the 24th International Cosmic Ray Conference, Rome, Italy*, edited by N. Iucci and E. Lamanna (International Union of Pure and Applied Physics, 1995), Vol. 1, p. 399, http://adsabs.harvard.edu/full/1995ICRC....1..399K.
[37] http://cosmos.n.kanagawa-u.ac.jp/EPICSHome.
[38] S. Roesler, R. Engel, and J. Ranft, in *Proceedings of the Monte Carlo Conference, Lisbon* (Springer, Berlin, Heidelberg, 2000), pp. 1033–1038, https://link.springer.com/chapter/10.1007%2F978-3-642-18211-2_166.
[39] A. Ferrari, P. R. Sala, A. Fassò, and J. Ranft, Technical Report CERN-2005-10, INFN/TC_05/11, SLAC-R-773, 2005.
[40] T. T. Böhlen, F. Cerutti, M. P. W. Chin, A. Fassò, A. Ferrari, P. G. Ortega, A. Mairani, P. R. Sala, G. Smirnov, and V. Vlachoudis, Nucl. Data Sheets **120**, 211 (2014).
[41] P. Maestro and N. Mori (CALET Collaboration), Proc. Sci., ICRC2017 (**2017**) 208, https://pos.sissa.it/301/208/pdf.
[42] P. S. Marrocchesi *et al.*, Nucl. Instrum. Methods Phys. Res., Sect. A **659**, 477 (2011).
[43] P. Maestro (CALET Collaboration), Adv. Space Res. **64**, 2538 (2019).
[44] See Supplemental Material at http://link.aps.org/supplemental/10.1103/PhysRevLett.125.251102 for supporting figures and the tabulated fluxes, as well as the description of data analysis procedure and the detailed assessment of systematic uncertainties.
[45] Y. Akaike (CALET Collaboration), Proc. Sci., ICRC2015 (**2015**) 613, https://pos.sissa.it/236/613/pdf.
[46] G. D'Agostini, Nucl. Instrum. Methods Phys. Res., Sect. A **362**, 487 (1995).
[47] T. Adye, arXiv:1105.1160.
[48] R. Brun and R. Rademarkers, Nucl. Instrum. Methods Phys. Res., Sect. A **389**, 81 (1997).
[49] Y. Akaike (CALET Collaboration), J. Phys. Conf. Ser. **1181**, 012042 (2019).
[50] J. J. Engelmann *et al.* (CREAM Collaboration), Astron. Astrophys. **233**, 96 (1990), http://articles.adsabs.harvard.edu/pdf/1990A%26A...233...96E.
[51] D. Müller, S. P. Swordy, P. Meyer, J. L'Heureux, and J. M. Grunsfeld, Astrophys. J. **374**, 356 (1991).
[52] O. Adriani *et al.* (PAMELA Collaboration), Astrophys. J. **93**, 791 (2014).
[53] E. Atkin *et al.* (NUCLEON Collaboration), J. Cosmol. Astropart. Phys. 07 (2017) 020.
[54] M. Simon, H. Spiegelhauer, W. K. H. Schmidt, F. Siohan, J. F. Ormes, V. K. Balasubrahmanyan, and J. F. Arens, Astrophys. J. **239**, 712 (1980).
[55] M. Ave *et al.* (TRACER Collaboration), Astrophys. J. **678**, 262 (2008).
[56] A. Panov *et al.* (ATIC Collaboration), Bull. Russ. Acad. Sci. **73**, 564 (2009).
[57] H. S. Ahn *et al.* (CREAM Collaboration), Astrophys. J. **707**, 593 (2009).